



TIDE : Temporal-Aware Sparse Autoencoders for Interpretable Diffusion Transformers in Image Generation

Victor Shea-Jay Huang^{1,2,*}, Le Zhuo^{1,2,*}, Yi Xin^{2,3}, Zhaokai Wang^{2,4}, Peng Gao², Hongsheng Li^{1†}
¹CUHK, MMLab ²Shanghai AI Laboratory ³NJU ⁴SJTU
jeix782@gmail.com, hsli@ee.cuhk.edu.hk

Abstract

Diffusion Transformers (DiTs) are a powerful yet underexplored class of generative models compared to U-Net-based diffusion models. To bridge this gap, we introduce TIDE (Temporal-aware Sparse Autoencoders for Interpretable Diffusion transformERS), a novel framework that enhances temporal reconstruction within DiT activation layers across denoising steps. TIDE employs Sparse Autoencoders (SAEs) with a sparse bottleneck layer to extract interpretable and hierarchical features, revealing that diffusion models inherently learn hierarchical features at multiple levels (e.g., 3D, semantic, class) during generative pre-training. Our approach achieves state-of-the-art reconstruction performance, with a mean squared error (MSE) of $1e-3$ and a cosine similarity of 0.97, demonstrating superior accuracy in capturing activation dynamics along the denoising trajectory. Beyond interpretability, we showcase TIDE's potential in downstream applications such as sparse activation-guided image editing and style transfer, enabling improved controllability for generative systems. By providing a comprehensive training and evaluation protocol for DiTs, TIDE contributes to the development of more interpretable, transparent, and trustworthy generative models.

1. Introduction

Recent advancements in diffusion models have revolutionized text-to-image generation, with Diffusion Transformers (DiTs) [43] emerging as a scalable alternative to traditional U-Net backbones [48] by leveraging transformer-based architectures. Improvements in sampling efficiency [60] and model scaling [5, 7, 14, 17, 62].

have further elevated their performance to a new level. However, a critical question remains: how do these models function internally? While interpretability techniques have been extensively developed for U-Net frameworks [28, 58], similar efforts for DiTs are absent. More broadly, interpretability research on diffusion models lags significantly

behind that of GANs [4, 18, 32], despite the growing prominence of diffusion models in generative modeling. This gap largely stems from diffusion models' reliance on latent space transformations across various denoising levels, which complicates efforts to analyze their internal mechanisms. In particular, little attention has been paid to understanding latent activations within these models, leaving a significant void in our ability to interpret their processes.

Feature interpretability, which aims to uncover how neural networks encode functionality through internal representations [13], has seen notable success in language models, especially through the use of sparse autoencoders (SAEs) [39]. These tools disentangle polysemantic neurons into sparse, human-interpretable features [6, 37]. However, existing SAE methods face significant limitations when applied to diffusion models, particularly at the level of activation layers. Diffusion models present unique challenges due to their temporal dynamics: unlike language models, which process static tokens in an auto-regressive manner, DiTs iteratively refine latent representations across timesteps, integrating multimodal inputs from text encoders. This iterative nature introduces difficulties such as long token sequences, high token dimensionality, and time-varying activation patterns, especially for high-resolution images. Similarly, although SAEs have proven effective in vision-language models [10] and convolutional networks [19], they encounter distinct challenges in DiTs, including:

1. Capturing time-varying activation patterns across diffusion steps;
2. Balancing sparsity and reconstruction fidelity during iterative denoising;
3. Aligning sparse features with both visual and text-conditioned semantics.

These challenges underscore the need for new interpretability methods tailored to the temporal and multimodal complexities of DiTs with SAE.

To address these issues, we present Temporal-aware SAEs for Interpretable Diffusion transformERS (TIDE), a framework designed to capture temporal variations in ac-

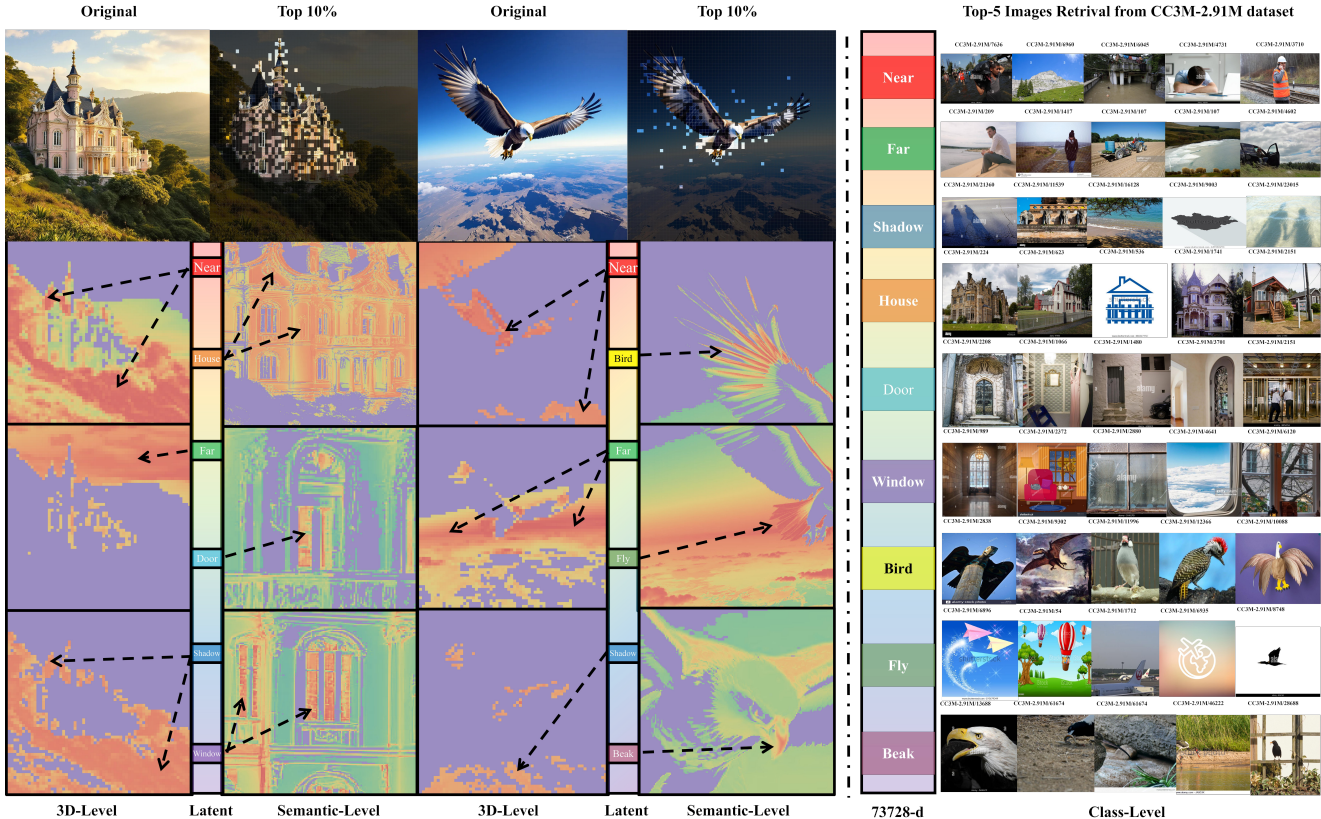


Figure 1. TIDE effectively encodes interpretable features across different levels (class, semantic, and 3D) in pre-trained diffusion transformer [7]. This validates that the diffusion model inherently captures and organizes these multi-level concepts by large-scale generative pre-training, enabling it to perform various downstream diffusion tasks effectively (see Sec. 5.4 for details).

tivation patterns and extract sparse, interpretable features throughout the denoising process. To ensure high-fidelity feature learning under sparsity constraints, we introduce specialized training strategies, including progressive sparsity scheduling and random sampling augmentation. Additionally, we explore TIDE’s scaling laws and validate its performance using diffusion loss, demonstrating that TIDE achieves state-of-the-art results compared to other SAE-based methods. Moreover, TIDE effectively learns multi-level features (e.g., 3D, semantics, and class), as shown in Fig. 1, highlighting how diffusion models inherently organize such concepts through large-scale generative pre-training. This finding illustrates their ability to be adapted to various downstream tasks, such as depth estimation [20, 25], semantic segmentation [57], and image classification [30, 38]. Additionally, we propose a temporal analysis that isolates and interprets the roles of individual timesteps in the generation process, offering deeper insights into the latent representations of text-conditioned image synthesis. By tailoring SAEs to the dynamics of DiTs, TIDE advances model interpretability, enhances understanding of generative mechanisms, and lays the foundation for more trustworthy and controllable generative sys-

tems.

This paper presents the first systematic study of SAEs in DiT-based diffusion models. Our contributions are fourfold:

- **TIDE Framework** (Sec 4.4): A paradigm that adapts SAEs to DiT via temporal-aware architecture and progressive sparsity scheduling, coupled with training strategies to extract interpretable features from DiT’s latent space while preserving generation quality and balancing sparsity with denoising efficacy.
- **Scaling Law and Evaluation** (Sec 5.3): We analyze the scaling law of TIDE, highlighting its ease of training, and compare its downstream loss with other SAEs to demonstrate the superior performance of TIDE.
- **Interpretation** (Sec 5.4 5.5): Using TIDE, we demonstrated that diffusion models learn hierarchical features through generative pre-training, enabling efficient transfer to target domains via fine-tuning. Furthermore, through a decoupled analysis of sampling timesteps, we verify and extend existing understanding about DiT’s Coarse-to-Fine generation.
- **Potential Applications** (Sec 6): Using PixArt- α [7], we demonstrate the practical utility of TIDE-learned sparse features in tasks like image editing and style transfer.

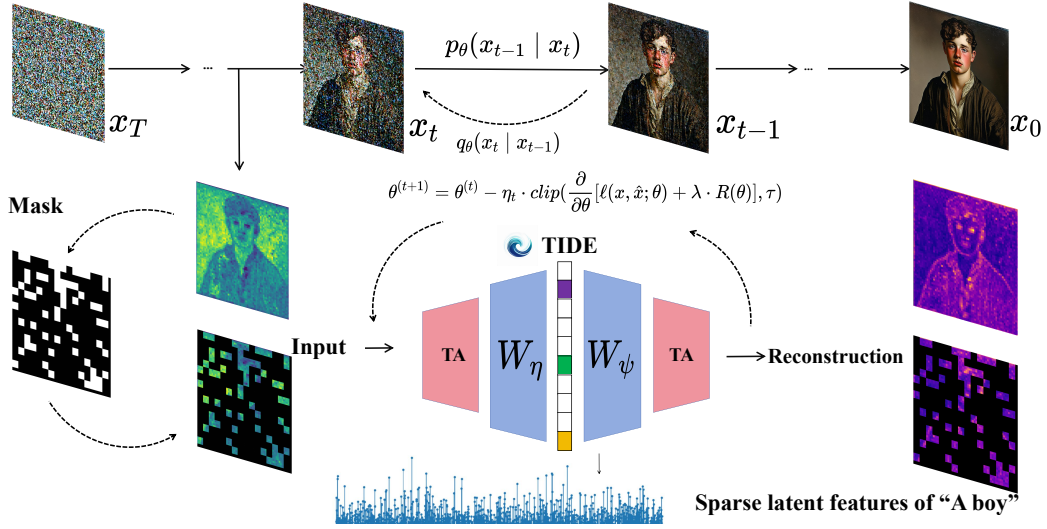


Figure 2. Overview of our training process: For each Dit, we train its TIDE individually, extracting activation layers from different timesteps each time. The training of the SAE is conducted using both with and without random sampling. For specific details on the loss design, refer to Sec. 4.3.

2. Related work

2.1. Sparse Autoencoders for Interpretability

Mechanistic interpretability [13] aims to understand how neural networks produce outputs by identifying features encoded in neurons [40]. Sparse autoencoders (SAEs)[41] address the polysemantic nature of neurons caused by superposition, where networks encode more features than dimensions[12, 49], by enforcing sparsity, activating only a small subset of neurons per input. SAEs have proven effective in uncovering human-interpretable features [6, 22], decomposing activations in large language models (LLMs)[56, 61], and extracting interpretable concepts in vision-language models such as CLIP[9]. They have also facilitated image editing [10], enabled concept naming [46], and disabled specific generative features [6], demonstrating their potential to mitigate superposition and enhance interpretability across diverse model architectures.

2.2. Interpretability of Diffusion Models

Diffusion models achieve text-to-image generation via iterative denoising, evolving from U-Net architectures [44, 47] to scalable designs like Diffusion Transformer (DiT) [43], with improved sampling efficiency [35, 51, 52]. Interpretability efforts focus on bottleneck layers [28, 42] and cross-attention [55], enabling manipulation of attributes [2] and text encoders [58]. SAEs, applied to CLIP [15, 45] and diffusion models [23, 26, 53], help identify features, reduce hallucinations [24], and analyze activations, linking features to visual semantics.

For more details on related work, please refer to the supplementary material.

3. Preliminaries

3.1. Sparse Autoencoder

To encode the extracted activations into a sparse latent representation, we employ a k -sparse autoencoder. The encoder and decoder are defined as follows:

$$\begin{aligned} l &= \text{ReLU}(W_{\text{enc}}a + b_{\text{enc}}), \\ \hat{a} &= W_{\text{dec}}l, \end{aligned} \quad (1)$$

where the encoder weights $W_{\text{enc}} \in \mathbb{R}^{n \times f}$, encoder bias $b_{\text{enc}} \in \mathbb{R}^n$, and decoder weights $W_{\text{dec}} \in \mathbb{R}^{f \times n}$ define the parameters of the autoencoder. Here, $a \in \mathbb{R}^f$ is the input vector, $l \in \mathbb{R}^n$ is the latent feature representation, and $\hat{a} \in \mathbb{R}^f$ is the reconstructed vector.

3.2. TopK Activation

We employ the k -sparse autoencoder [36], which uses the TopK activation function to enforce sparsity. This function selects the k largest latent activations and sets the rest to zero. The function is defined as:

$$z = \text{TopK}(l), \quad (2)$$

where $l \in \mathbb{R}^n$ is the latent feature representation. The decoder remains unchanged.

As shown in [16], TopK activation offers several advantages: it directly enforces sparsity by controlling the number of active units, eliminating the need for ℓ_1 regularization; simplifies model comparison by avoiding hyperparameter tuning; improves sparsity-reconstruction trade-offs, especially in larger models; and enhances feature interpretability by zeroing out small activations.

3.3. Diffusion Transformer

Diffusion Transformers (DiT) [43] are transformer-based diffusion models designed for latent space, achieving competitive performance in image generation tasks. Unlike traditional diffusion models that utilize U-Net backbones, DiT employs transformer architectures to process latent patches, offering improved scalability and efficiency. Within the latent diffusion model (LDM) [47] framework, images are first compressed into latent representations via a variational autoencoder (VAE) [27], and then a transformer models the denoising process, reducing computational complexity while preserving output quality.

The forward diffusion process follows a Markov chain, sequentially adding Gaussian noise. At timestep t , the noisy data x_t is formulated as:

$$x_t = \sqrt{\bar{\alpha}_t}x_0 + \sqrt{1 - \bar{\alpha}_t}\epsilon_t, \quad \epsilon_t \sim \mathcal{N}(0, \mathbf{I}), \quad (3)$$

where $\bar{\alpha}_t$ defines the noise schedule. The reverse process, modeled by the transformer, predicts noise $\epsilon_\theta(x_t)$ to iteratively denoise x_t . The training objective minimizes the mean squared error between predicted and true noise:

$$L_{\text{simple}}(\theta) = \mathbb{E}_{x_0, \epsilon_t, t} [\|\epsilon_\theta(x_t) - \epsilon_t\|^2]. \quad (4)$$

DiT’s scalable architecture and strong performance on benchmarks like ImageNet position it as a state-of-the-art model for high-resolution image generation.

4. Methodology

4.1. Where to Train Sparse Autoencoders (SAEs)

Recent research on the mechanistic interpretability of diffusion models [2, 3] has revealed that distinct cross-attention blocks are responsible for generating particular visual elements, including style and objects. Using these insights, since diffusion models share similar architectures, we selected a representative model, **PixArt-XL-2-1024-MS** [7], to extract activation layers for training SAEs. A dedicated SAE was trained for each activation layer. The training process is in Fig. 2

4.2. Activations in DiTs

To enable the use of latent activations from diffusion models for training SAEs, activations are extracted from specific transformer layers during both the forward diffusion and reverse denoising processes.

Given an input image \mathbf{x}_0 and a text prompt \mathbf{p} , the image is encoded into the latent space \mathbf{z}_0 using a VAE encoder. Noise ϵ is added to simulate the diffusion process, producing a noisy latent \mathbf{z}_t at timestep t . Simultaneously, the text prompt is embedded into \mathbf{e}_p via a text encoder. The noisy latent \mathbf{z}_t and text embedding \mathbf{e}_p are fed into the transformer

Algorithm 1 Activation Extraction

Require: Image \mathbf{x}_0 , Text \mathbf{p} , Time step t , DiTs \mathcal{T} , Target layer ℓ

Ensure: Activations \mathbf{a}_ℓ

- 1: Encode image: $\mathbf{z}_0 \leftarrow f_{\text{enc}}(\mathbf{x}_0)$
 - 2: Sample noise: $\epsilon \sim \mathcal{N}(0, \mathbf{I})$
 - 3: Add noise: $\mathbf{z}_t \leftarrow \sqrt{\bar{\alpha}_t}\mathbf{z}_0 + \sqrt{1 - \bar{\alpha}_t}\epsilon$
 - 4: Encode text: $\mathbf{e}_p \leftarrow f_{\text{text}}(\mathbf{p})$
 - 5: Register hook at layer ℓ : $g_\ell : \mathbf{a}_\ell = \phi_\ell(\mathbf{u}_\ell)$
 - 6: Forward pass: $\mathbf{h}_{\text{out}} \leftarrow \mathcal{T}(\mathbf{z}_t, \mathbf{e}_p, t)$
 - 7: Extract activations: $\mathbf{a}_\ell \leftarrow g_\ell(\mathbf{u}_\ell)$
 - 8: **return** \mathbf{a}_ℓ
-

model, where hooks capture activations from specified layers during the forward pass. These activations are then used to train SAEs.

This approach leverages intermediate representations from the generation pipeline for downstream tasks. The activation extraction process is detailed in Algorithm 1.

4.3. Training Loss

The optimization process updates the SAEs’ parameters θ iteratively using the following formula:

$$\theta^{(t+1)} = \theta^{(t)} - \eta_t \cdot \text{clip}\left(\mathbf{g}^{(t)}, \tau\right), \quad (5)$$

where η_t denotes the learning rate at step t , and $\mathbf{g}^{(t)}$ is the gradient of the training loss with respect to the SAEs’ parameters θ :

$$\mathbf{g}^{(t)} = \frac{\partial}{\partial \theta} [\ell(x, \hat{x}; \theta) + \lambda_{\text{reg}} \cdot R(\theta)]. \quad (6)$$

The training loss function $\ell(x, \hat{x}; \theta)$ consists of multiple components, each capturing a different aspect of the model’s performance. It is defined as:

$$\ell(x, \hat{x}; \theta) = \mathcal{L}_{\text{mse}} + \mathcal{L}_{\text{cos}} + \mathcal{L}_{\text{temporal}} + \mathcal{L}_{\text{spsa}}. \quad (7)$$

Our loss function balances reconstruction, temporal distribution and sparsity. For more details on training, please refer to the supplementary material.

4.4. TIDE: Temporal-Aware SAE

In our training process, we observed that directly reconstructing the activation layers of DiTs using a SAE yielded relatively favorable results. However, the convergence was still noticeably slow. Inspired by the timestep sampling mechanism in diffusion models, we introduce temporal information into the activation layers to enhance the representation of timestep-dependent features.

The inclusion of temporal information is motivated by the fact that the token distribution varies significantly across

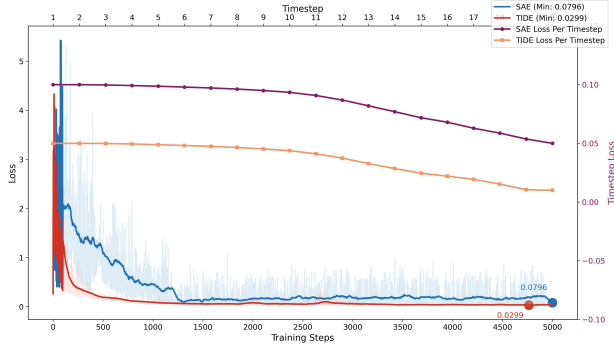


Figure 3. TIDE integrates timestep-dependent modulation into the original SAE architecture, achieving significantly faster convergence and enhanced performance.

different timesteps. For instance, at smaller timesteps (low t), the amount of information present is substantially different compared to larger timesteps (high t), where the input contains significant noise. To effectively disentangle these timestep-specific characteristics, it is crucial to inform the SAE of the corresponding timestep during reconstruction.

To address these timestep-dependent activation variations, we propose the Temporal-Aware SAE (TIDE), which incorporates a timestep-dependent modulation operation:

$$x_{\text{mod}} = x \cdot (1 + \text{scale}) + \text{shift}, \quad (8)$$

which is initialized from the pre-trained adaptive Layer Normalization in DiT.

As shown in Fig. 3, this modulation adjusts the activations by applying timestep-specific scaling and shifting, allowing the model to adapt to the varying distributions of activation layers across different timesteps. Building upon the Top-k SAE framework, the addition of this modulation mechanism enables TIDE to effectively handle timestep-dependent activation distributions without requiring substantial modifications to the SAE parameters.

To prevent dead latents—latent variables that cease to activate during training—we employ careful initialization and revival strategies. Specifically, the encoder is initialized as the transpose of the decoder, and any inactive latents are periodically revived throughout the training process.

5. Experiments

5.1. Training Setup

Each SAE/TIDE was carried out using three distinct strategies, with 40 hours of training on 8 A100 80G GPUs:

- **Direct Training:** Using 80K prompt-image pairs extracted from CC3M [50] without additional data augmentation.
- **Augmented Training:** To mitigate overly dense local features and reduce overfitting, we randomly sample 1/16 of

Train	MSE	S_{cos}	MSE^{val}	S_{cos}^{val}
SAE	$3.3e-3$	0.968	$1.23e-2$	0.935
SAE(sample)	$2.5e-3$	0.970	$1.26e-2$	0.962
TIDE	$3.1e-3$	0.970	$1.02e-2$	0.944
TIDE(sample)	$2.5e-3$	0.972	$1.02e-2$	0.964

Table 1. SAE ($d \times 16d$, sparsity 5%, Avg of 28 layers) training Results (with/without Sampling Strategy and TA Architecture).

the tokens at the token level for each activation layer. Furthermore, we use a consistent set of 80K pairs to control for the effects of the sampling operation.

- **TIDE Training:** Incorporating a *Temporal-Aware Architecture* (Sec 4.4) to enhance the model’s ability to capture temporal dynamics within the activation features.

Evaluation The performance of TIDE was evaluated using cosine similarity, mean squared error (MSE), and sparsity loss (see Sec 4.3 and the supplementary material). These metrics also guided the training process, ensuring that the TIDEs(SAEs) struck a balance between sparsity and reconstruction accuracy.

Hyperparameters The training process employed key hyperparameters (see the supplementary material for details), including token-level sampling rate, cosine annealing learning rate scheduler, and AdamW [34] optimizer with weight decay.

5.2. SAEs / TIDEs Exhibit Superior Reconstruction

We conducted experiments to evaluate the impact of token-level sampling during training and the addition of the temporal-aware architecture in PixArt’s 28 Diffusion Transformers (DiTs) activation layers. The results are summarized in Tab. 1. Our analysis reveals that, while the training strategy without sampling augment did not significantly improve performance on the reconstruction task, it led to a noticeable improvement in cosine similarity on the out-of-distribution (OOD) validation set relative to the training dataset, with only a minor increase in MSE.

This result reveals two key insights: **(1)** Using the same amount of training data, sampling reduces interference from global image features with only 1/16 of the total tokens, enabling more accurate extraction of critical features and thereby improving both reconstruction precision and generalization. **(2)** The minimal change in MSE suggests that the data norm remains stable, with only slight directional adjustments. This indicates that the activation distribution is largely preserved, and reconstructed activation layers have minimal impact on subsequent image generation quality.

Furthermore, incorporating the TA architecture provides slight improvements in both MSE and cosine similarity, enabling more accurate reconstructions even at the 10^{-3} scale. This can be attributed not only to the sufficiently large latent

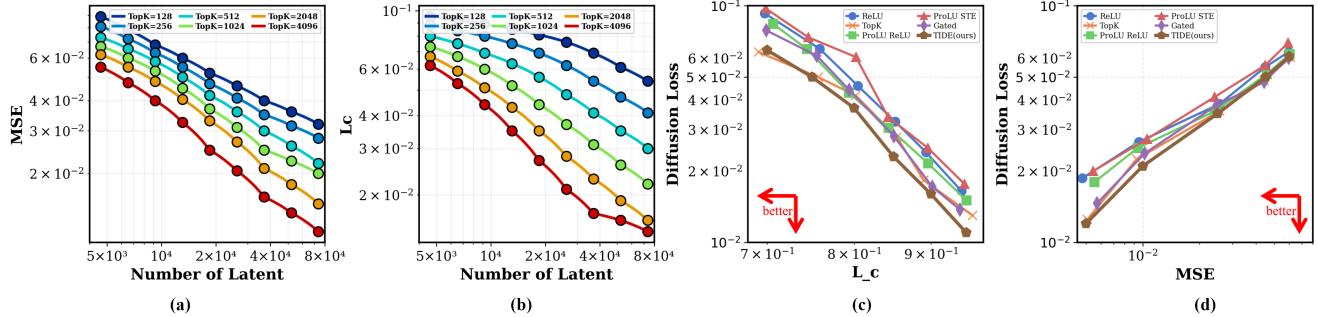


Figure 4. (a)(b) Scaling laws of convergence loss with fixed latents n under MSE and cosine similarity loss ($L_{cos} = 1 - S_{cos}$). (c)(d) Comparison of TIDE and other activation functions: For 73728-d latents, TIDE achieves better trade-offs in diffusion loss against both cosine similarity and MSE.

space and carefully designed sparsity but also to the alignment with the principle of time embedding-based sampling in diffusion models.

5.3. Scaling Laws and Downstream Loss of TIDEs

Given the broad capabilities of state-of-the-art (SoTA) diffusion models — distinct from large language models (LLMs) — diffusion models exhibit significantly higher feature dimensionality and process a large number of tokens in each operation. Consequently, we hypothesize that accurately capturing the state of the model requires a large number of sparse features. To address this, we propose two primary approaches for determining the size of the autoencoder and the token budget:

As shown in Fig. 4(a)(b), increasing the number of latent dimensions from $d = 4608$ to $16d = 73728$, along with a higher top-k selection, leads to progressively better reconstruction of the activation layers. This improvement is reflected in a MSE reaching the order of 10^{-3} and a cosine similarity approaching 0.97. Compared to other diffusion U-Net-based SAEs, as well as most SoTA LLM-based SAEs, the TIDEs trained using our strategy consistently achieve SoTA performance.

We use the downstream diffusion loss to evaluate the reconstruction quality of TIDE. Specifically, the activation layers reconstructed by TIDE are used to replace the original activation layers in DiT, and the diffusion loss is then calculated. As shown in Fig. 4(c)(d), the diffusion loss of TIDE’s reconstructed features is comparable to that of the original model and surpasses other types of SAEs, all while achieving SoTA performance. This highlights TIDE’s effectiveness in preserving features crucial to the generation task.

5.4. Diffusion Really Learned Features

Recent studies have demonstrated the versatility of diffusion models across a range of downstream tasks, including depth estimation, classification, and segmentation. This

raises two fundamental questions:

1. **Do diffusion models inherently encode the knowledge necessary for these tasks?**
2. **Can TIDE validate the existence of such representations, thereby demonstrating their potential to support downstream applications?**

To address these questions, we conducted a series of well-designed experiments to investigate the internal feature representations learned by diffusion models. For each target feature of interest, we selected 1K images containing identical target elements from a curated dataset optimized to minimize background interference and irrelevant semantic content. From these images, we extracted activations from the penultimate layer of the DiT model and applied average pooling to aggregate the latent features. Based on these pooled features, we computed similarity scores between the input image tokens and identified the top-k tokens with the highest similarity. The results, as illustrated in Fig. 1, demonstrate that TIDE effectively exploits the internal representations of DiT to extract multi-level features, which can be categorized as follows:

- **3D-Level:** TIDE captures features such as “far,” “near,” and “shadow,” which are indicative of spatial relationships and distinctions between the foreground and background. The activation patterns associated with these features exhibit a high degree of specificity, and training images with similar activations consistently share these characteristics. This consistency underscores the capacity of diffusion models to encode 3D-related concepts critical for downstream tasks like depth estimation.
- **Class-Level:** Beyond 3D-level information, TIDE learns class-level representations and their associated sub-features. For example, the class “Rococo” is characterized by sub-features such as “house,” “window,” and “door,” while “eagle” is defined by sub-features like “bird,” “fly,” and “beak.” These features demonstrate clear activation patterns localized within distinct regions of the input images, further validating the hierarchical organiza-

tion of the learned representations.

- **Semantic-Level:** Building on the class-level representations, TIDE isolates finer-grained semantic-level features and their corresponding spatial locations within images. For instance, it can precisely identify the “beak” of an eagle and its position within an image, showcasing the model’s ability to extract localized and semantically rich details.

As shown in Fig.1, these findings confirm that TIDE effectively encodes interpretable features at multiple levels—spanning 3D, class, and semantic representations—within pre-trained DiTs[7]. This analysis underscores the nuanced, hierarchical structure of features learned during large-scale generative pre-training, demonstrating that diffusion models inherently capture and organize multi-level concepts. It provides compelling evidence of their potential to support diverse downstream applications while laying a foundation for future advancements in practical tasks. Consequently, these features enable the models to excel in a variety of downstream tasks. For instance, the ability to capture class-level and semantic-level representations underpins the model’s suitability for tasks like classification [30, 38] and segmentation, as evidenced by zero-shot, unsupervised approaches such as Diff-Seg [57]. Similarly, the capability to learn 3D-related concepts empowers diffusion models to tackle depth estimation challenges effectively, as demonstrated by SoTA methods like Marigold [25] for single-image depth prediction and DepthFM [20] for rapid monocular depth estimation.

5.5. Coarse-to-fine Generation in DiT

Based on our TIDE and the results shown in Fig. 5, we observed in the interpretable latent space that, from the perspective of sparse feature activation, abrupt changes in both cosine similarity and MSE metrics are concentrated at the timestep when contours are formed, indicating that this moment marks a critical transition where the latent space begins aligning the original image manifold with the target manifold. This phenomenon not only supports the hypothesis of a “coarse-to-fine” generation process but also suggests that the entire denoising process may involve a transition between two sampling modes. A similar perspective is discussed in [11], where it highlights a potential connection between diffusion models and autoregressive models, suggesting that diffusion models essentially perform an approximate form of autoregression in the frequency domain. Specifically, the iterative denoising process in diffusion models can be interpreted as a low-pass filtering operation, where noise gradually overwhelms high-frequency signals while preserving low-frequency structures, progressively recovering image details through spectral decomposition. This frequency-domain perspective further explains the “coarse-to-fine” behavior observed during image gener-

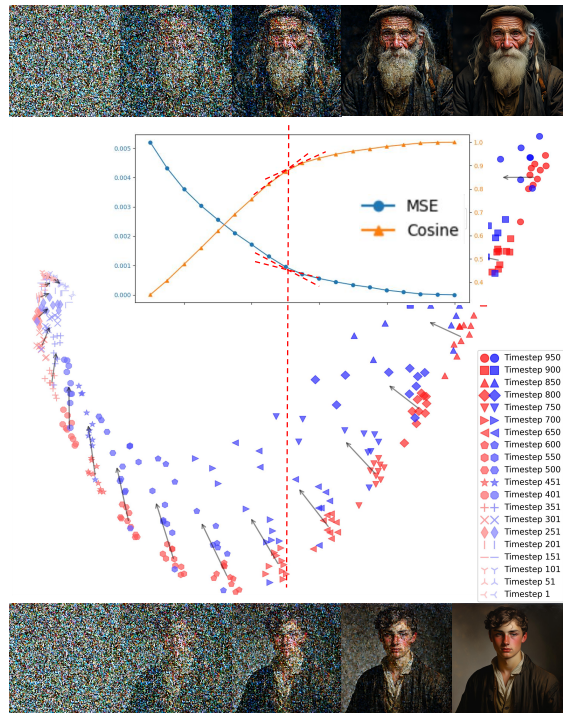


Figure 5. The generation progress shows that at each timestep, DiT’s activation layers form a directed vector connecting latent features to target features. Abrupt changes in cosine similarity and MSE mark the timestep when contours emerge, signaling the alignment of the latent space with the target manifold. Early modifications aid alignment, while later ones refine details. Using this, we reconstruct latent representations and guide modifications with a directed vector at each step.

ation in diffusion models, aligning closely with our findings from sparse feature activation, and provides additional insights into the generative logic of diffusion models.

6. Potential Application

Based on the analysis in the previous section, we choose to modify the activation layer of the penultimate DiT, which has a significant impact on the output. As shown in Fig. 5, for each timestep, there always exists a directed vector between the latent feature and the target feature. At this point, the significance of Self-Attention Embedding is also reflected. By modifying the TIDE latent feature, we not only achieve better interpretability but also avoid out-of-distribution (OOD) errors caused by directly operating on the activation layer. Additionally, we can add the classifier-free guidance (CFG) Renormalization [31], as shown in the formula below, to ensure the stability of the norm.

$$\tilde{F}_\theta(x_t, c_T, c_I, t) = \frac{\hat{F}_\theta(x_t, c_T, c_I, t) \|F_\theta(x_t, c_T, c_I, t)\|}{\|\hat{F}_\theta(x_t, c_T, c_I, t)\|} \quad (9)$$



Figure 6. By manipulating the latent space of the TIDE, we can achieve various concept transformations, such as erasing Rococo style, increasing age, and altering the orientation and shape of architecture. The extent of feature modification intensifies as the number of altered tokens increases.

The interpretable latent space enables various modification strategies, such as erasing or inverting top-K features to remove fine details, scaling activation indices to achieve feature transitions, or directly replacing latent features for global changes. These approaches can produce diverse effects, as shown in Fig. 6.

TIDE-based image editing methods, while not yet matching the performance of certain highly optimized traditional approaches — such as GANs or domain-specific pre-trained models — in scenarios requiring exceptionally high-quality edits, offer distinct advantages that address key limitations of conventional techniques. Traditional methods, often reliant on prompt-based operations, can produce high-quality results but struggle with limited interpretability, insufficient control over polysemantics, and susceptibility to unpredictable outputs. In contrast, TIDE leverages sparse feature extraction and modification, enabling precise control, stability, and transparency in the editing process while providing detailed insights into the model’s internal mechanisms. These strengths make TIDE particularly valuable in applications where precision, reliability, and interpretability are critical, such as medical image modification or ensuring accountability throughout the generation process. Furthermore, TIDE extends its utility beyond image editing by guiding model optimization, reducing bias, and fostering the development of innovative generative techniques, establishing a foundation for more trustworthy technologies.

7. Limitations

Current SAE-based image editing methods still face challenges in achieving high-quality edits in complex scenarios. These limitations may stem from insufficient feature representation capacity due to the sparsity constraints of the model. Future work will focus on optimizing the design of sparsity constraints and exploring dynamic sparse activation mechanisms to improve editing quality while maintaining interpretability and stability.

8. Conclusion

This work presents a systematic exploration of interpretability in diffusion models, with a focus on DiTs. Through the introduction of the TIDE framework, we explore the unique temporal dynamics of DiTs, proposing novel training strategies, sparsity scheduling, and a decoupled analysis of the generation process. Our findings explore scaling law for TIDE, demonstrate its SoTA performance compared to other SAEs, and highlight its ability to learn hierarchical features during generative pre-training, enabling efficient transfer to downstream tasks. Furthermore, comprehensive experiments validate the practical utility of TIDE-learned sparse features in applications such as image editing and style transfer. By advancing the transparency, controllability, and interpretability of DiTs, this work provides a foundation for building more trustworthy generative systems, while also offering new directions for future research in understanding diffusion-based architectures.

TIDE : Temporal-Aware Sparse Autoencoders for Interpretable Diffusion Transformers in Image Generation

Supplementary Material

A. Related work

A.1. Sparse Autoencoders for Interpretability

Mechanistic interpretability [13] aims to uncover how neural networks produce their outputs by identifying the features or concepts encoded within individual neurons [40]. A key challenge arises from the polysemantic nature of neurons [12], where a single neuron can respond to multiple unrelated concepts due to superposition, a phenomenon in which neural networks encode more features than they have dimensions [12, 49]. Sparse autoencoders (SAEs) [41] address this issue by learning compact and interpretable representations through a sparsity-constrained latent space, where only a small subset of neurons activates for each input.

Recent advancements demonstrate the effectiveness of SAEs in mechanistic interpretability, enabling the discovery of human-interpretable features [6, 22] and sparse feature circuits in language models [37]. SAEs have been applied to decompose activations in large language models (LLMs), revealing features related to biases and safety that can be manipulated to steer model behavior [8, 56, 61]. Similarly, in vision-language models such as CLIP [45], SAEs have been used to extract interpretable concepts from the vision encoder [9] and facilitate image editing in diffusion models [10]. Furthermore, SAEs have enabled concept naming via embeddings from the CLIP text encoder for concept bottleneck models [46] and have been employed to disable specific generative features in text-to-image diffusion models. These applications highlight the potential of SAEs to mitigate superposition and enhance interpretability across diverse model architectures.

A.2. Interpretability of Diffusion Models

Diffusion models have shown remarkable performance in text-to-image (T2I) generation by iteratively predicting Gaussian noise within latent representations. Early implementations relied on U-Net architectures [44, 47], but recent advancements have introduced the more scalable Diffusion Transformer (DiT) [43], as demonstrated in works such as [5, 7, 29, 33, 59, 62]. Improvements in sampling efficiency [35, 51, 52, 60] have further enhanced image quality while reducing computational costs. Despite these advances, interpretability studies on diffusion models remain limited.

Efforts to interpret U-Net-based models have focused on disentangling semantic directions in bottleneck layers [21, 28, 42] and analyzing cross-attention mechanisms [55]. For example, [2, 3] demonstrated how attributes could be manipulated by adjusting text inputs at specific layers, while [58] interpreted text encoders by generating intermediate image outputs. Sparse autoencoders (SAEs), widely used in language models, have seen limited adoption in vision tasks. Early applications include manipulating CLIP representations [10, 15, 45] and traditional convolutional networks [19, 54]. More recently, SAEs have been employed in vision-language models to reduce hallucinations [24] and to enhance radiology reporting [1]. In T2I diffusion models, SAEs have been used to identify meaningful features in bottleneck layers [23], distill knowledge from SDXL-Turbo blocks [53], and analyze unconditional sampling activations across timesteps [26], linking features with visual semantics.

B. Training design

B.1. Training Loss

The optimization process updates the parameters of the stacked autoencoders (SAEs) θ iteratively using the following formula:

$$\theta^{(t+1)} = \theta^{(t)} - \eta_t \cdot \text{clip}(\mathbf{g}^{(t)}, \tau) \quad (10)$$

where η_t denotes the learning rate at step t , and $\mathbf{g}^{(t)}$ is the gradient of the training loss with respect to the model's parameters θ . The gradient $\mathbf{g}^{(t)}$ is computed as:

$$\mathbf{g}^{(t)} = \frac{\partial}{\partial \theta} [\ell(x, \hat{x}; \theta) + \lambda_{\text{reg}} \cdot R(\theta)] \quad (11)$$

Here, $\ell(x, \hat{x}; \theta)$ defines the training loss, and $R(\theta)$ is the regularization term. The parameter λ_{reg} controls the strength of regularization.

The training loss $\ell(x, \hat{x}; \theta)$ consists of multiple components, each of which captures a specific aspect of the model’s performance. It is expressed as:

$$\ell(x, \hat{x}; \theta) = \mathcal{L}_{\text{mse}} + \mathcal{L}_{\text{cos}} + \mathcal{L}_{\text{temporal}} + \mathcal{L}_{\text{spa}} \quad (12)$$

- **Reconstruction Loss:** The reconstruction loss \mathcal{L}_{mse} measures the mean squared error (MSE) between the input x and its reconstruction \hat{x} :

$$\mathcal{L}_{\text{mse}} = \lambda_{\text{mse}} \|x - \hat{x}\|_2^2 \quad (13)$$

- **Cosine Similarity Loss:** The cosine similarity loss \mathcal{L}_{cos} ensures directional alignment between x and \hat{x} by minimizing the cosine distance:

$$\mathcal{L}_{\text{cos}} = \lambda_{\text{cos}} \left(1 - \frac{\mathbf{x} \cdot \hat{\mathbf{x}}}{\|\mathbf{x}\| \|\hat{\mathbf{x}}\|} \right) \quad (14)$$

- **Temporal Consistency Loss:** The temporal consistency loss $\mathcal{L}_{\text{temporal}}$ enforces smoothness across time steps in sequential data:

$$\mathcal{L}_{\text{temporal}} = \lambda_{\text{temporal}} \|F_t - F_{t+1}\|_2^2 \quad (15)$$

- **Sparsity Loss:** The sparsity loss \mathcal{L}_{spa} promotes sparse representations in the latent space. It is implemented using the Huber loss:

$$\mathcal{L}_{\text{spa}} = \lambda_{\text{spa}} \begin{cases} \frac{1}{2}(S - S_{\text{target}})^2 & \text{if } |S - S_{\text{target}}| \leq \delta \\ \delta|S - S_{\text{target}}| - \frac{1}{2}\delta^2 & \text{otherwise} \end{cases} \quad (16)$$

B.2. Regularization

To prevent overfitting and ensure well-posed optimization, the loss function includes a regularization term $R(\theta)$, defined as:

$$R(\theta) = \|W_{\text{encoder}}\|_2^2 + \|W_{\text{decoder}}\|_2^2 \quad (17)$$

where W_{encoder} and W_{decoder} denote the weights of the encoder and decoder, respectively. The L_2 norm is applied to penalize large weights, ensuring model stability and generalizability.

B.3. Gradient Clipping

To stabilize the optimization process and mitigate the risk of gradient explosion, gradient clipping is employed. The clipping function $\text{clip}(\mathbf{g}, \tau)$ is defined as:

$$\text{clip}(\mathbf{g}, \tau) = \begin{cases} \mathbf{g}, & \|\mathbf{g}\| \leq \tau, \\ \frac{\tau}{\|\mathbf{g}\|} \cdot \mathbf{g}, & \|\mathbf{g}\| > \tau \end{cases} \quad (18)$$

where $\|\mathbf{g}\|$ represents the norm of the gradient vector. When the gradient norm exceeds the threshold τ , the gradient is scaled down to have a norm equal to τ . This ensures that updates remain controlled, improving the stability of the convergence.

C. Potential Application

Based on the analysis in the previous section, we propose a novel strategy to modify the activation layer of the penultimate DiT (Diffusion Transformer), which significantly influences the output. As illustrated in Fig.5 in the main text, for every timestep, a directed vector exists between the latent feature and the target feature. This relationship highlights the importance of the Self-Attention Embedding in achieving meaningful feature alignment. By operating on the TIDE latent feature — rather than directly on the activation layer — we not only enhance the interpretability of the process but also mitigate the risk of out-of-distribution (OOD) errors. To ensure numerical stability during these operations, we introduce classifier-free guidance (CFG) Renormalization [31], as expressed in the formula below:

$$\tilde{F}_\theta(x_t, c_T, c_I, t) = \frac{\hat{F}_\theta(x_t, c_T, c_I, t) \cdot \|F_\theta(x_t, c_T, c_I, t)\|}{\|\hat{F}_\theta(x_t, c_T, c_I, t)\|}, \quad (19)$$

where:

- \tilde{F}_θ represents the renormalized TIDE latent feature.

- \hat{F}_θ is the modified latent feature after applying feature editing operations.
- F_θ denotes the original latent feature before modification.
- x_t is the input at timestep t .
- c_T and c_I represent the text and image conditions, respectively.

This renormalization ensures that the norm of the modified latent feature \hat{F}_θ is scaled to match the norm of the original feature F_θ , maintaining numerical stability and preventing extreme deviations during editing. By normalizing the modified feature, we ensure that the edits remain consistent with the model’s expected latent space dynamics.

C.1. Modification Strategies

The interpretable latent space introduced by TIDE enables various modification strategies. These strategies are designed to offer fine-grained control over edits while maintaining stability:

- **Erasing or Inverting Top-K Features:** By selectively erasing or inverting the top-K features of the original latent feature while preserving the overall norm, we can alter the direction of these features. This approach allows us to remove fine-grained details, as shown in the first row of Fig. 6, where intricate rococo-style elements are erased, leaving behind only the basic background and structural attributes of a house. This operation offers a baseline for more sophisticated modifications.
- **Scaling Activation Indices:** By scaling the top-K activation indices of the target latent feature within the original latent feature, we can achieve smooth transitions and gradual feature changes. For example, in the second row of Fig. 6, this technique is used to progressively add aging attributes to the image of a young boy, resulting in a controlled transformation.
- **Global Replacement of Latent Features:** A more aggressive editing strategy involves directly replacing the original latent feature with the target latent feature at a specific timestep. This method can produce dramatic global modifications, as illustrated in the third row of Fig. 6.

These diverse strategies showcase the flexibility of TIDE in image editing and its ability to achieve fine control over both local and global transformations.

C.2. Advantages of TIDE-Based Methods

Although TIDE-based image editing methods may not yet rival the performance of highly optimized traditional approaches — such as GANs or domain-specific pre-trained models — in tasks requiring extremely high-quality image edits, they offer several unique advantages over conventional techniques:

- **Enhanced Interpretability:** Traditional methods, often reliant on prompt-based operations, struggle to fully interpret the multi-faceted semantics of individual features. Outputs are frequently influenced by unanticipated factors, making these methods less transparent. TIDE, by contrast, provides a clear understanding of the internal mechanisms of the generative model, empowering users to make informed modifications.
- **Precise Control:** Through sparse feature extraction and targeted modification, TIDE enables precise control over editing outcomes. This ensures that users can achieve their desired results without compromising model stability or generating unintended artifacts.
- **Stability and Transparency:** TIDE’s reliance on well-defined latent space operations ensures consistent and predictable outputs, making it a reliable tool for scenarios where accountability and trustworthiness are critical.
- **Broader Applicability:** Beyond image editing, TIDE’s interpretability-focused framework has potential applications in areas such as model optimization, bias reduction, and the development of innovative generative techniques. For example, TIDE-based methods can guide the refinement of generative models or help identify and mitigate biases in generated content.

C.3. Application Scenarios

The combination of interpretability, precision, and stability makes TIDE particularly valuable in scenarios requiring high levels of control and trustworthiness:

- **Medical Image Editing:** In medical imaging, where precision and accountability are paramount, TIDE’s interpretability ensures that modifications are both accurate and transparent, reducing the risk of errors in critical applications such as diagnostics or surgical planning.
- **Creative Industries:** TIDE’s ability to edit fine details and achieve gradual transformations makes it a versatile tool for tasks such as artistic rendering, style transfer, or content creation.
- **Model Optimization and Bias Reduction:** By offering insights into the internal workings of generative models, TIDE can guide efforts to optimize model performance and address issues such as bias or fairness in AI-generated content.

References

- [1] Ahmed Abdulaal, Hugo Fry, Nina Montaña-Brown, Ayodeji Ijishakin, Jack Gao, Stephanie Hyland, Daniel C Alexander, and Daniel C Castro. An x-ray is worth 15 features: Sparse autoencoders for interpretable radiology report generation. *arXiv preprint arXiv:2410.03334*, 2024. 1
- [2] Samyadeep Basu, Nanxuan Zhao, Vlad I Morariu, Soheil Feizi, and Varun Manjunatha. Localizing and editing knowledge in text-to-image generative models. In *The Twelfth International Conference on Learning Representations*, 2023. 3, 4, 1
- [3] Samyadeep Basu, Keivan Rezaei, Priyatham Kattakinda, Vlad I Morariu, Nanxuan Zhao, Ryan A Rossi, Varun Manjunatha, and Soheil Feizi. On mechanistic knowledge localization in text-to-image generative models. In *Forty-first International Conference on Machine Learning*, 2024. 4, 1
- [4] David Bau, Jun-Yan Zhu, Hendrik Strobelt, Bolei Zhou, Joshua B Tenenbaum, William T Freeman, and Antonio Torralba. Gan dissection: Visualizing and understanding generative adversarial networks. *arXiv preprint arXiv:1811.10597*, 2018. 1
- [5] James Betker, Gabriel Goh, Li Jing, Tim Brooks, Jianfeng Wang, Linjie Li, Long Ouyang, Juntang Zhuang, Joyce Lee, Yufei Guo, et al. Improving image generation with better captions. *Computer Science*. <https://cdn.openai.com/papers/dall-e-3.pdf>, 2(3):8, 2023. 1
- [6] Trenton Bricken, Adly Templeton, Joshua Batson, Brian Chen, Adam Jermy, Tom Conerly, Nick Turner, Cem Anil, Carson Denison, Amanda Askell, Robert Lasenby, Yifan Wu, Shauna Kravec, Nicholas Schiefer, Tim Maxwell, Nicholas Joseph, Zac Hatfield-Dodds, Alex Tamkin, Karina Nguyen, Brayden McLean, Josiah E Burke, Tristan Hume, Shan Carter, Tom Henighan, and Christopher Olah. Towards monosemanticity: Decomposing language models with dictionary learning. *Transformer Circuits Thread*, 2023. <https://transformer-circuits.pub/2023/monosemantic-features/index.html>. 1, 3
- [7] Junsong Chen, Jincheng Yu, Chongjian Ge, Lewei Yao, Enze Xie, Yue Wu, Zhongdao Wang, James Kwok, Ping Luo, Huchuan Lu, et al. Pixart- α : Fast training of diffusion transformer for photorealistic text-to-image synthesis. *ICLR*, 2023. 1, 2, 4, 7
- [8] Hoagy Cunningham, Aidan Ewart, Logan Riggs, Robert Huben, and Lee Sharkey. Sparse autoencoders find highly interpretable features in language models. *arXiv preprint arXiv:2309.08600*, 2023. 1
- [9] Gytis Daujotas. Interpreting and steering features in images, 2024. 3, 1
- [10] Gytis Daujotas. Case study: Interpreting, manipulating, and controlling clip with sparse autoencoders, 2024. 1, 3
- [11] Sander Dieleman. Diffusion is spectral autoregression, 2024. 7
- [12] Elhage, Nelson, Hume, Tristan, Olsson, Catherine, Schiefer, Nicholas, Henighan, Tom, Kravec, Shauna, Hatfield-Dodds, Zac, Lasenb, Robert, Drain, Dawn, Chen, Carol, et al. Toymodelsof superposition. 2022. 3, 1
- [13] Nelson Elhage, Neel Nanda, Catherine Olsson, Tom Henighan, Nicholas Joseph, Ben Mann, Amanda Askell, Yuntao Bai, Anna Chen, Tom Conerly, Nova DasSarma, Dawn Drain, Deep Ganguli, Zac Hatfield-Dodds, Danny Hernandez, Andy Jones, Jackson Kernion, Liane Lovitt, Kamal Ndousse, Dario Amodei, Tom Brown, Jack Clark, Jared Kaplan, Sam McCandlish, and Chris Olah. A mathematical framework for transformer circuits, 2021. *Anthropic*. 1, 3
- [14] Patrick Esser, Sumith Kulal, Andreas Blattmann, Rahim Entezari, Jonas Müller, Harry Saini, Yam Levi, Dominik Lorenz, Axel Sauer, Frederic Boesel, et al. Scaling rectified flow transformers for high-resolution image synthesis. 2024. 1
- [15] Hugo Fry. Towards multimodal interpretability: Learning sparse interpretable features in vision transformers, 2024. 3, 1
- [16] Leo Gao, Tom Dupré la Tour, Henk Tillman, Gabriel Goh, Rajan Troll, Alec Radford, Ilya Sutskever, Jan Leike, and Jeffrey Wu. Scaling and evaluating sparse autoencoders. *arXiv preprint arXiv:2406.04093*, 2024. 3
- [17] Peng Gao, Le Zhuo, Dongyang Liu, Ruoyi Du, Xu Luo, Longtian Qiu, Yuhang Zhang, Rongjie Huang, Shijie Geng, Renrui Zhang, et al. Lumina-t2x: Scalable flow-based large diffusion transformer for flexible resolution generation. In *The Thirteenth International Conference on Learning Representations*. 1
- [18] Ian Goodfellow, Jean Pouget-Abadie, Mehdi Mirza, Bing Xu, David Warde-Farley, Sherjil Ozair, Aaron Courville, and Yoshua Bengio. Generative adversarial nets. *Advances in neural information processing systems*, 27, 2014. 1
- [19] Liv Gorton. The missing curve detectors of inceptionv1: Applying sparse autoencoders to inceptionv1 early vision. *arXiv preprint arXiv:2406.03662*, 2024. 1
- [20] Ming Gui, Johannes Schusterbauer, Ulrich Prestel, Pingchuan Ma, Dmytro Kotovenko, Olga Grebenkova, Stefan Andreas Baumann, Vincent Tao Hu, and Björn Ommer. Depthfm: Fast monocular depth estimation with flow matching. *arXiv preprint arXiv:2403.13788*, 2024. 2, 7
- [21] Jaehoon Hahm, Junho Lee, Sunghyun Kim, and Joonseok Lee. Isometric representation learning for disentangled latent space of diffusion models. In *International conference on machine learning*, 2024. 1
- [22] Robert Huben, Hoagy Cunningham, Logan Riggs Smith, Aidan Ewart, and Lee Sharkey. Sparse autoencoders find highly interpretable features in language models. In *The Twelfth International Conference on Learning Representations*, 2024. 3, 1
- [23] Ayodeji Ijishakin, Ming Liang Ang, Levente Baljer, Daniel Chee Hian Tan, Hugo Laurence Fry, Ahmed Abdulaal, Aengus Lynch, and James H Cole. H-space sparse autoencoders. In *Neurips Safe Generative AI Workshop 2024*, 2024. 3, 1
- [24] Nick Jiang, Anish Kachinthaya, Suzie Petryk, and Yossi Gandelsman. Interpreting and editing vision-language representations to mitigate hallucinations. *arXiv preprint arXiv:2410.02762*, 2024. 3, 1

- [25] Bingxin Ke, Anton Obukhov, Shengyu Huang, Nando Metzger, Rodrigo Caye Daudt, and Konrad Schindler. Repurposing diffusion-based image generators for monocular depth estimation. In *Proceedings of the IEEE/CVF Conference on Computer Vision and Pattern Recognition*, pages 9492–9502, 2024. 2, 7
- [26] Dahye Kim, Xavier Thomas, and Deepti Ghadiyaram. *Revelio*: Interpreting and leveraging semantic information in diffusion models. *arXiv preprint arXiv:2411.16725*, 2024. 3, 1
- [27] Diederik P Kingma, Max Welling, et al. Auto-encoding variational bayes, 2013. 4
- [28] Mingi Kwon, Jaeseok Jeong, and Youngjung Uh. Diffusion models already have a semantic latent space. In *The Eleventh International Conference on Learning Representations*, 2023. 1, 3
- [29] Black Forest Labs. Flux. <https://github.com/black-forest-labs/flux>, 2024. 1
- [30] Alexander C Li, Mihir Prabhudesai, Shivam Duggal, Ellis Brown, and Deepak Pathak. Your diffusion model is secretly a zero-shot classifier. In *Proceedings of the IEEE/CVF International Conference on Computer Vision*, pages 2206–2217, 2023. 2, 7
- [31] Zongyu Lin, Wei Liu, Chen Chen, Jiasen Lu, Wenzhe Hu, Tsu-Jui Fu, Jesse Allardice, Zhengfeng Lai, Liangchen Song, Bowen Zhang, et al. Stiv: Scalable text and image conditioned video generation. *arXiv preprint arXiv:2412.07730*, 2024. 7, 2
- [32] Huan Ling, Karsten Kreis, Daiqing Li, Seung Wook Kim, Antonio Torralba, and Sanja Fidler. Editgan: High-precision semantic image editing. *Advances in Neural Information Processing Systems*, 34:16331–16345, 2021. 1
- [33] Dongyang Liu, Shicheng Li, Yutong Liu, Zhen Li, Kai Wang, Xinyue Li, Qi Qin, Yufei Liu, Yi Xin, Zhongyu Li, et al. Lumina-video: Efficient and flexible video generation with multi-scale next-dit. *arXiv preprint arXiv:2502.06782*, 2025. 1
- [34] Ilya Loshchilov and Frank Hutter. Decoupled weight decay regularization. *arXiv preprint arXiv:1711.05101*, 2017. 5
- [35] Cheng Lu, Yuhao Zhou, Fan Bao, Jianfei Chen, Chongxuan Li, and Jun Zhu. Dpm-solver: A fast ode solver for diffusion probabilistic model sampling in around 10 steps. *NeurIPS*, 35:5775–5787, 2022. 3, 1
- [36] Alireza Makhzani and Brendan Frey. K-sparse autoencoders. *arXiv preprint arXiv:1312.5663*, 2013. 3
- [37] Samuel Marks, Can Rager, Eric J Michaud, Yonatan Belinkov, David Bau, and Aaron Mueller. Sparse feature circuits: Discovering and editing interpretable causal graphs in language models. *arXiv preprint arXiv:2403.19647*, 2024. 1
- [38] Soumik Mukhopadhyay, Matthew Gwilliam, Vatsal Agarwal, Namitha Padmanabhan, Archana Swaminathan, Srinidhi Hegde, Tianyi Zhou, and Abhinav Shrivastava. Diffusion models beat gans on image classification. *arXiv preprint arXiv:2307.08702*, 2023. 2, 7
- [39] Andrew Ng et al. Sparse autoencoder. *CS294A Lecture notes*, 72(2011):1–19, 2011. 1
- [40] Chris Olah, Nick Cammarata, Ludwig Schubert, Gabriel Goh, Michael Petrov, and Shan Carter. Zoom in: An introduction to circuits. *Distill*, 5(3):e00024–001, 2020. 3, 1
- [41] Bruno A. Olshausen and David J. Field. Sparse coding with an overcomplete basis set: A strategy employed by v1? *Vision Research*, 37:3311–3325, 1997. 3, 1
- [42] Yong-Hyun Park, Mingi Kwon, Jaewoong Choi, Junghyo Jo, and Youngjung Uh. Understanding the latent space of diffusion models through the lens of riemannian geometry. *Advances in Neural Information Processing Systems*, 36:24129–24142, 2023. 3, 1
- [43] William S Peebles and Saining Xie. Scalable diffusion models with transformers. In *ICCV*, 2022. 1, 3, 4
- [44] Dustin Podell, Zion English, Kyle Lacey, Andreas Blattmann, Tim Dockhorn, Jonas Müller, Joe Penna, and Robin Rombach. Sdxl: Improving latent diffusion models for high-resolution image synthesis. *arXiv preprint arXiv:2307.01952*, 2023. 3, 1
- [45] Alec Radford, Jong Wook Kim, Chris Hallacy, Aditya Ramesh, Gabriel Goh, Sandhini Agarwal, Girish Sastry, Amanda Askell, Pamela Mishkin, Jack Clark, et al. Learning transferable visual models from natural language supervision. In *International conference on machine learning (ICLR)*, pages 8748–8763. PMLR, 2021. 3, 1
- [46] Sukrut Rao, Sweta Mahajan, Moritz Böhle, and Bernt Schiele. Discover-then-name: Task-agnostic concept bottlenecks via automated concept discovery. *arXiv preprint arXiv:2407.14499*, 2024. 3, 1
- [47] Robin Rombach, Andreas Blattmann, Dominik Lorenz, Patrick Esser, and Björn Ommer. High-resolution image synthesis with latent diffusion models. In *Proceedings of the IEEE/CVF conference on computer vision and pattern recognition*, pages 10684–10695, 2022. 3, 4, 1
- [48] Olaf Ronneberger, Philipp Fischer, and Thomas Brox. U-net: Convolutional networks for biomedical image segmentation. In *Medical image computing and computer-assisted intervention—MICCAI 2015: 18th international conference, Munich, Germany, October 5-9, 2015, proceedings, part III 18*, pages 234–241. Springer, 2015. 1
- [49] Lee Sharkey, Dan Braun, and beren. Taking features out of superposition with sparse autoencoders, 2022. AI Alignment Forum. 3, 1
- [50] Piyush Sharma, Nan Ding, Sebastian Goodman, and Radu Soricut. Conceptual captions: A cleaned, hypernymed, image alt-text dataset for automatic image captioning. In *Proceedings of ACL*, 2018. 5
- [51] Jiaming Song, Chenlin Meng, and Stefano Ermon. Denoising diffusion implicit models. *arXiv preprint arXiv:2010.02502*, 2020. 3, 1
- [52] Yang Song and Stefano Ermon. Generative modeling by estimating gradients of the data distribution. *NeurIPS*, 32, 2019. 3, 1
- [53] Viacheslav Surkov, Chris Wendler, Mikhail Terekhov, Justin Deschenaux, Robert West, and Caglar Gulcehre. Unpacking sdxl turbo: Interpreting text-to-image models with sparse autoencoders. *arXiv preprint arXiv:2410.22366*, 2024. 3, 1
- [54] Christian Szegedy, Wei Liu, Yangqing Jia, Pierre Sermanet, Scott Reed, Dragomir Anguelov, Dumitru Erhan, Vincent Vanhoucke, and Andrew Rabinovich. Going deeper with convolutions. In *Proceedings of the IEEE conference on computer vision and pattern recognition*, pages 1–9, 2015. 1

- [55] Raphael Tang, Linqing Liu, Akshat Pandey, Zhiying Jiang, Gefei Yang, Karun Kumar, Pontus Stenetorp, Jimmy Lin, and Ferhan Ture. What the daam: Interpreting stable diffusion using cross attention. *arXiv preprint arXiv:2210.04885*, 2022. 3, 1
- [56] Adly Templeton. *Scaling monosemanticity: Extracting interpretable features from claude 3 sonnet*. Anthropic, 2024. 3, 1
- [57] Junjiao Tian, Lavisha Aggarwal, Andrea Colaco, Zsolt Kira, and Mar Gonzalez-Franco. Diffuse attend and segment: Unsupervised zero-shot segmentation using stable diffusion. In *Proceedings of the IEEE/CVF Conference on Computer Vision and Pattern Recognition*, pages 3554–3563, 2024. 2, 7
- [58] Michael Toker, Hadas Orgad, Mor Ventura, Dana Arad, and Yonatan Belinkov. Diffusion lens: Interpreting text encoders in text-to-image pipelines. *arXiv preprint arXiv:2403.05846*, 2024. 1, 3
- [59] Enze Xie, Junsong Chen, Junyu Chen, Han Cai, Haotian Tang, Yujun Lin, Zhekai Zhang, Muyang Li, Ligeng Zhu, Yao Lu, et al. Sana: Efficient high-resolution image synthesis with linear diffusion transformers. *ICLR*, 2025. 1
- [60] Mingyang Yi, Aoxue Li, Yi Xin, and Zhenguo Li. Towards understanding the working mechanism of text-to-image diffusion model. *NeurIPS*, 2024. 1
- [61] Zeyu Yun, Yubei Chen, Bruno A Olshausen, and Yann LeCun. Transformer visualization via dictionary learning: contextualized embedding as a linear superposition of transformer factors. *arXiv preprint arXiv:2103.15949*, 2021. 3, 1
- [62] Le Zhuo, Ruoyi Du, Han Xiao, Yangguang Li, Dongyang Liu, Rongjie Huang, Wenze Liu, Lirui Zhao, Fu-Yun Wang, Zhanyu Ma, et al. Lumina-next: Making lumina-t2x stronger and faster with next-dit. *NeurIPS*, 2024. 1